

# Helium variation in Four Small Magellanic Cloud Globular Clusters<sup>1</sup>

Edoardo P. Lagioia, Antonino P. Milone, Anna F. Marino

*Dipartimento di Fisica e Astronomia “Galileo Galilei”*

*Università di Padova, Vicolo dell’Osservatorio 3, I-35122, Padua, Italy*

edoardo.lagioia@unipd.it

and

Aaron Dotter

*Harvard-Smithsonian Center for Astrophysics, Cambridge, MA 02138, USA*

## ABSTRACT

The multiple stellar populations (MPs) of the  $\sim 11$ -13 Gyr-old Globular Clusters (GCs) in our Galaxy are characterized by different content of several light elements. These elements describe well-defined patterns like the C-N and the Na-O anticorrelations and the He-N and Na-N correlations.

The discovery of the MPs in Magellanic Cloud GCs opened up new paths for the investigation of chemical anomalies in clusters with different age and physical properties.

In this context, we used *Hubble Space Telescope* photometry to investigate the MPs and constrain their chemical composition of four  $\sim 6$ -11 Gyr extragalactic GCs, namely NGC 121, NGC 339, NGC 416 and Lindsay 1 in the Small Magellanic Cloud.

The comparison of the stellar colors with synthetic spectra suggests that second-population stars of NGC 121, NGC 339, NGC 416 are slightly enhanced in helium by  $\delta Y = 0.009 \pm 0.006$ ,  $0.007 \pm 0.004$  and  $0.010 \pm 0.003$ , respectively, with respect to the first population, while we find no significant helium variation in Lindsay 1 ( $\delta Y = 0.000 \pm 0.004$ ). Moreover, second-population stars of all the clusters are, on average, enhanced in nitrogen and depleted in carbon and oxygen, in close analogy with what we observe in Galactic GCs.

*Subject headings:* stars: abundances — globular clusters: general — globular clusters: individual(NGC 121, NGC 339, NGC 416, Lindsay 1)

## 1. Introduction

The observation of multiple populations (MPs) in the old ( $\sim 11$ -13 Gyr) Globular Clusters (GCs) of our Galaxy sets a new standard in the definition of the nature of these objects. Previously thought to be composed of a single, coeval generation of stars, GCs in fact host distinct groups of stars with chemical properties characterized by specific patterns defined by the anti-

correlation of the light elements C-N and Na-O (Kraft 1994; Gratton et al. 2012), the difference in helium content and, in some cases, by metallicity variations (Marino et al. 2015). In this regard, the determination of internal helium variations among GC stars is of primary importance because it provides compelling information about the physical processes that led to the formation of MPs (Decressin et al. 2007; D’Ercole et al. 2008; Bastian et al. 2013; D’Antona et al. 2016); allows to constrain models of stellar structure and evolution (Cassisi et al. 2017); ultimately, gives impor-

<sup>1</sup>Accepted for publication on ApJ, 06 December 2018

tant clues about the role played by the first stars in the reionization of the Universe at high-redshift (Schaerer & Charbonnel 2011; Renzini 2017).

Direct spectroscopic measurements of absolute helium abundance in old GCs, however, are limited to hot horizontal branch (HB) stars in the effective temperature ( $T_{\text{eff}}$ ) range 8,000-11,500 K (e.g. Villanova et al. 2009; Marino et al. 2014). In hotter stars, indeed, the pristine atmospheric chemical composition is altered by radiative levitation of metals and gravitational settling of helium (Grundahl et al. 1999; Behr 2003; Moehler et al. 2004). In addition, for some GCs, spectroscopic helium estimates have been derived from chromospheric lines of few stars at the Red Giant Branch (RGB) tip (Pasquini et al. 2011; Dupree et al. 2011).

Relative helium variations between MPs in a GC can be estimated, instead, for a large number of stars. An increase in helium content results, in fact, in a larger  $T_{\text{eff}}$  hence in a color change, at a given luminosity, for stars along the Main Sequence (MS) and the RGB. Several works, based on *Hubble Space Telescope* (*HST*) multi-wavelength photometry, have used this property to infer the difference in helium mass fraction ( $\delta Y$ ) in MPs of about 60 Galactic GCs with a precision better than 0.01 (Milone et al. 2012a; Milone 2015; Milone et al. 2018a).

Helium variations affect also the stellar luminosities and, as a consequence, the location of the characteristic evolutionary features in a color-magnitude diagram (CMD). In particular, the brightness of the RGB Bump (RGBB) is directly related to the helium content of the underlying stellar population (see Cassisi et al. 1997, and references therein). This implies that any difference in luminosity between the RGBBs of distinct populations in a monometallic (same  $[M/H]$ ) GC can be used to infer their relative helium content. Recent analyses have provided the first  $\delta Y$  estimates from the RGBB of MPs for a sample of about 20 Galactic GCs (Lee 2015; Milone et al. 2015a; Lee 2017; Lagioia et al. 2018; Lee 2018).

Both helium and light-element variations are crucial observational constraints to test the validity of any proposed theory of formation of MPs in GCs. The observed chemical patterns, indeed, suggest that MPs are the result of internal enrichment processes according to which secondary gen-

erations of stars form in an intracluster medium polluted with material processed and ejected from the pristine stellar generation (see Renzini et al. 2015, and references therein). Since the formation of the subsequent stellar generations occurs at the very early stages of cluster life and, therefore, in different physical conditions, the search for signature of the presence of MPs in clusters with different age and in different environment is of primary importance.

While the relative helium abundance of MPs has been investigated in a large number of Galactic GCs, the helium content of MPs in extragalactic GCs is still unexplored. In this respect, the GCs in the Magellanic Clouds represent a valuable statistical sample. These extragalactic systems, indeed, are close enough to be resolved into single stars and span a wide range of ages, going from few Myrs to  $\sim 11$  Gyr (e.g. Johnson et al. 1999; Bertelli et al. 2003; Mackey & Gilmore 2004; Glatt et al. 2008a,b).

In the last years several works have been dedicated to the study of MPs in the Magellanic Cloud GCs. While clusters older than  $\sim 2$  Gyr exhibit light-element variations and multiple RGBs in CMDs obtained with ultraviolet filters (e.g. Mucciarelli et al. 2009; Dalessandro et al. 2016; Niederhofer et al. 2017a,b; Martocchia et al. 2018), clusters younger than  $\sim 2$  Gyr do not show any star-to-star abundance variations (Mucciarelli et al. 2011, 2014) but, rather, some peculiar photometric features, namely split MS and/or extended MS turn-off, which can be interpreted as due to age spread caused by prolonged star formation episodes (e.g. Mackey & Broby Nielsen 2007; Mackey et al. 2008; Goudfrooij et al. 2009; Milone et al. 2009; Goudfrooij et al. 2011) or to a difference in rotational velocity of MS stars (e.g. D’Antona et al. 2015; Bastian et al. 2016; Milone et al. 2016, 2017a, 2018b).

In this paper we will exploit multi-band *HST* photometry to infer, for the first time, the helium content of MPs in four  $\sim 6$ -11 Gyr-old Small Magellanic Cloud (SMC) GCs, namely NGC 121, NGC 339, and NGC 416 and Lindsay 1 (Dalessandro et al. 2016; Niederhofer et al. 2017a,b). The paper is organized as follows. In Section 2 we describe the data and the procedure to derive photometry and astrometry. The multiple populations are identified in Section 3, while

Sections 4 and 5 are devoted to the determination of the helium abundance from the colors of RGB stars and from the magnitudes of the RGBBs, respectively. Summary and discussion are provided in Section 6.

## 2. Observations and data reduction

For our analysis we took advantage of archival<sup>2</sup> *HST* observations of NGC 121, NGC 339, NGC 416 and Lindsay 1. In particular we used images collected with WFC3/UVIS in the UV bands F336W and F343N and in the optical band F438W, and with ACS/WFC in the optical bands F555W and F814W. For NGC 121, the dataset also includes F814W images collected with WFC3/UVIS. A summary of the observations used in this work is provided in Table 1.

The photometric analysis performed on all the images and already described in Milone et al. (2018b), is summarized hereafter. We performed the data reduction on *flt* images that, in the case of UV observations, were previously corrected for the poor charge-transfer efficiency following the recipe of Anderson & Bedin (2010). For each image, we computed a  $5 \times 5$  array of perturbed point-spread functions (PSFs), starting from library empirical PSFs and, then, adding spatial-variation corrections obtained from unsaturated and isolated bright stars. To obtain the position and flux of bright stars we employed *img2xym* (Anderson & King 2006), a computer program suitably developed for the reduction of *HST* data, which is also able to identify saturated stars and accurately determine their magnitude, by taking into account the amount of flux bled into adjacent pixels (Gilliland 2004; Anderson et al. 2008; Gilliland 2010). The position and flux of faint stars was, instead, obtained with a different program (Anderson et al. in preparation), that takes into account all the images in which a stellar image is present. Specifications about the algorithm employed by this program are provided in Sabbi et al. (2016) and Bellini et al. (2017).

We calibrated the instrumental magnitudes to the VEGAMAG system following the method of Bedin et al. (2005), using the UVIS and WFC encircled energy distribution and the photometric

zero points available at the STScI website<sup>3</sup>. The position of stars was also corrected for geometric distortion by using the solution of Bellini et al. (2011) and transformed to the Gaia DR1 reference system (Gaia Collaboration et al. 2016).

Finally, we selected for our analysis all the stars measured with high photometric accuracy, by employing the quality indexes provided with the software, according to the method detailed in Milone et al. (2009).

The resulting  $m_{F814W}$  vs.  $m_{F555W} - m_{F814W}$  CMDs of the four GCs are shown in Figure 1. In all the cases, we employed the F555W and F814W magnitudes obtained from ACS observations and displayed all the stars within 1000 ACS/WFC pixels ( $\sim 50$  arcsec) from the cluster center. Indeed, since our analysis is aimed at determining the average helium difference of the two main stellar populations in each GC, we need to select the bulk of cluster members, which are distributed in the innermost region around the cluster center. Moreover, the adoption of the same radius for all the GCs derives from the fact that all the clusters have approximately the same distance modulus (Glatt et al. 2008a,b). However we verified that the conclusions of our work are not affected by such an assumption. Therefore, the following analysis is only referred to the sub-sample of stars included in the aforementioned radial selection.

### 2.1. Artificial Stars

Artificial stars (ASs) were obtained to generate synthetic color-color diagrams and compare them with observations. The adopted AS test, described in detail in Anderson et al. (2008) is briefly summarized here. For each GC we created a list of  $5 \times 10^5$  ASs, including coordinates and magnitudes, distributed along the fiducial line of cluster. Then, for each AS in the list, we generated a star with appropriate position and flux and applied the same procedure and PSF model, used for real stars, to obtain the photometry of the star. We also used the same diagnostics employed for the selection of real stars to assess the photometric and astrometric quality of the ASs. Finally, we selected only relatively isolated ASs, with small astrometric and photometric errors, and well fitted

<sup>2</sup><https://archive.stsci.edu/>

<sup>3</sup>[http://www.stsci.edu/hst/wfc3/analysis/uviz\\_zpts/](http://www.stsci.edu/hst/wfc3/analysis/uviz_zpts/),  
<http://www.stsci.edu/hst/acs/analysis/zeropoints>

TABLE 1  
OBSERVATION DATASET.

Cluster	date	camera	filter	No.×exposure time (s)	Proposal ID
NGC 121	21 Jan 2006	ACS/WFC	F555W	$2 \times 20 + 4 \times 496$	10396
			F814W	$2 \times 10 + 4 \times 474$	
	16 May 2014, 16 Oct 2014	WFC3/UVIS	F336W	$4 \times 1061$	13435
			F438W	$4 \times 200$	
			F814W	$2 \times 100$	
NGC 339	01 May 2016	ACS/WFC	F343N	$500 + 800 + 1650$	14069
	28 Nov 2005		F555W	$2 \times 20 + 4 \times 496$	10396
	08 Aug 2016	WFC3/UVIS	F814W	$2 \times 10 + 4 \times 474$	14069
			F336W	$700 + 1160 + 1200$	
			F343N	$520 + 800 + 1250 + 1650$	
NGC 416	22 Nov 2005, 08 Mar 2006	ACS/WFC	F438W	$120 + 180 + 560 + 660$	10396
			F814W	$4 \times 10 + 4 \times 474$	
	08 Mar 2006, 16 Jun 2016	WFC3/UVIS	F555W	$2 \times 20 + 4 \times 496$	14069
			F336W	$700 + 1160 + 1200$	
			F343N	$500 + 800 + 1650 + 1655$	
Lindsay 1	11 Jul 2003, 21 Aug 2005	ACS/WFC	F438W	$120 + 180 + 560 + 660$	9891, 10396
			F814W	$2 \times 10 + 290 + 4 \times 474$	
	19 Jun 2016	WFC3/UVIS	F336W	$500 + 2 \times 1200$	14069
			F343N	$500 + 800 + 1650 + 1850$	
			F438W	$120 + 2 \times 460$	

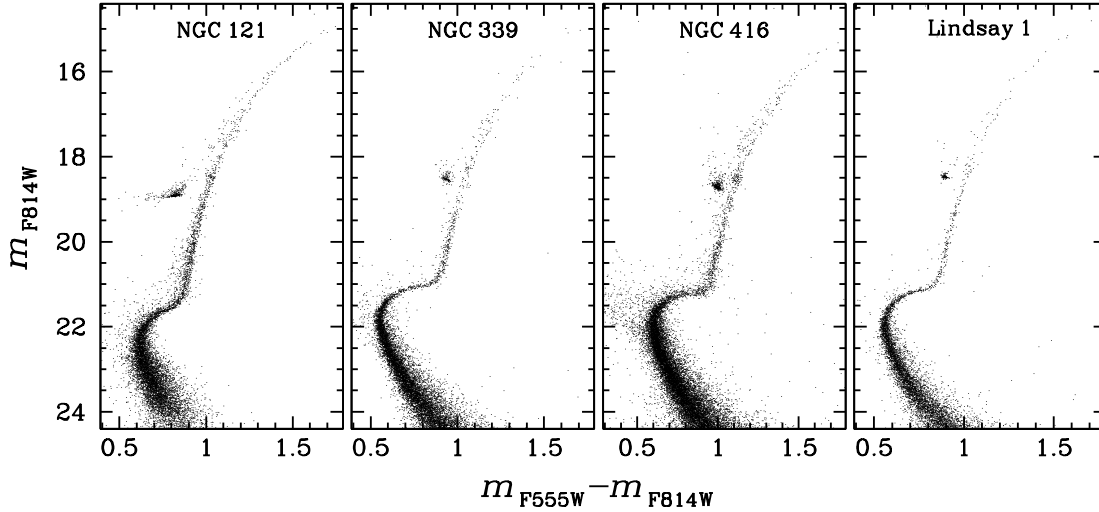


Fig. 1.—  $m_{F814W}$  vs.  $m_{F555W} - m_{F814W}$  CMDs of the four GCs analyzed in this work. For each cluster only stars within  $\sim 50$  arcsec from the cluster center are displayed.

by the adopted PSF model.

### 3. Multiple populations along the RGB

A glance at the plots in Fig. 1 reveals that every CMD is compatible with a single stellar population. However, recent works have shown that, when observed in UV-optical CMDs, all the analyzed GCs display a split (NGC 121, Dalessandro et al. 2016; Niederhofer et al. 2017a) or a broadened (NGC 339, NGC 416, Lindsay 1 Niederhofer et al. 2017b) RGB, suggesting the presence of multiple populations. At variance with pure optical colors indeed, colors obtained from an appropriate combinations of UV, optical and near-infrared bands are ideal for the detection of stellar populations characterized by different chemical content (Marino et al. 2008; Milone et al. 2012b, 2013; Monelli et al. 2014).

For this reason, we devised a procedure for the selection of the MPs along the RGB of each analyzed cluster, based on the comparison of the distribution of the observed and artificial stars in the  $m_{F336W} - m_{F555W}$  vs  $C_{F343N, F438W, F814W}$  pseudo color-color diagram, with  $C_{F343N, F438W, F814W} = (m_{F343N} - m_{F438W}) - (m_{F438W} - m_{F814W})$ .

We empirically verified that this diagram maximizes the separation of the RGB stars with different chemical content. It exploits, indeed, the property of the narrow UV filter F343N, whose transmission curve is centered on the absorption band of the NH molecule, and of the F336W and F438W filters, which are similar to the Johnson broadband filters  $U$  and  $B$  and are sensitive to the nitrogen and carbon content, respectively<sup>4</sup>. We also note in passing that  $C_{F343N, F438W, F814W}$  is similar to the color index  $c_{UBI}$  for the Johnson-Cousin filter system (Milone et al. 2012a; Monelli et al. 2013).

An example of the procedure, applied to the case of NGC 121, is given in Figure 2, where in panel (a) is shown the  $m_{F814W}$  vs.  $m_{F438W} - m_{F814W}$  CMD of the cluster, with the RGB mem-

bers represented as dark gray points. The selection of the RGB sample was done by considering the location of ‘bona-fide’ RGB stars in the  $m_{F555W}$  vs.  $m_{F336W} - m_{F555W}$  and in the  $m_{F814W}$  vs.  $m_{F438W} - m_{F814W}$  CMD of the cluster. Owing to low statistics we excluded stars in the proximity of the RGB tip. All the stars flagged as ‘bona-fide’ RGB stars in both the CMDs were considered RGB members.

We show, in panel (b), the  $m_{F336W} - m_{F555W}$  vs  $C_{F343N, F438W, F814W}$  color-color diagram of the selected RGB members. In this diagram the stars seem to be distributed into two different groups, elongated approximately in the upper-left bottom-right direction, for  $m_{F336W} - m_{F555W}$  colors redder than  $\sim 1$ . Similarly, in panel (c), we show the same pseudo color-color diagram but for the RGB members of the AS sample. Since the ASs were generated, by construction, using ideal evolutionary sequences represented by the fiducial lines, their dispersion in the mentioned pseudo color-color diagram is indicative of the color dispersion that we would ideally observe for a single stellar population.

With the aim of comparing the color dispersion of the observed and artificial stars, we divided  $m_{F336W} - m_{F555W}$  color range in a regular grid of  $C_i$  points  $w/3$  mag apart and, for each point, computed the 10th percentile of the distribution of the  $C_{F343N, F438W, F814W}$  values of all the stars in the interval  $(m_{F336W} - m_{F555W}) - w/2 < C_i < (m_{F336W} - m_{F555W}) + w/2$  (Silverman 1986). Finally, we linearly interpolated the resulting points. We used a binwidth  $w = 0.25$  for NGC 121 and NGC 416,  $w = 0.35$  for NGC 339 and  $w = 0.40$  for Lindsay 1.

We applied the same procedure for the ASs, but this time we also computed the points corresponding to the 98th percentile of the distribution of the  $C_{F343N, F438W, F814W}$  values. The  $C_{F343N, F438W, F814W}$  values of the ASs have been then translated so that the line interpolating the 10th-percentile points of the ASs overlapped that of the observed points.

We have represented the interpolating function of the 10th-percentile points of the observed stars as a solid line connecting the black dots in panel (b) and (c), and the interpolating function of the 98th-percentile points function as the solid line connecting the black triangles in

<sup>4</sup>The choice of the  $m_{F336W} - m_{F555W}$  vs  $C_{F343N, F438W, F814W}$  color-color diagram to select the two cluster stellar populations, rather than the  $m_{F814W}$  vs  $C_{F343N, F438W, F814W}$  pseudo CMD, is also justified by two additional reasons: the sensitivity of the  $m_{F336W} - m_{F555W}$  index to the nitrogen stellar content through the band F336W (see e.g. Milone et al. 2012b); the independent information provided by the two color indices  $m_{F336W} - m_{F555W}$  and  $C_{F343N, F438W, F814W}$ .

panel (c) and panel (d). As visible in the latter panel, the 98th-percentile line divides the observed stars into two groups, that we will conventionally name PopA and PopB. We observe that PopA stars, represented as red points, attain on average  $C_{F343N,F438W,F814W}$  values bluer than PopB stars, represented as blue points.

The adopted convention was chosen in analogy to the results obtained from the comparison of the spectroscopic and photometric features of Red Giants in Galactic GCs, where Na-poor (O-rich) RGB stars have lower  $c_{UBI}$  values than Na-rich (O-poor) RGB stars (e.g. Monelli et al. 2013; Marino et al. 2017). For the same reason, we expect that PopB stars are enhanced in He, N, Na and depleted in C and O, with respect to PopA stars. In the rest of the paper we will use the same color-code to represent all the quantities related to PopA and PopB stars.

As already mentioned, we applied the previous method to identify the two main stellar populations along the RGB of every cluster analyzed in this work. Figure 3 displays, for each labeled GC, the  $m_{F336W} - m_{F555W}$  vs  $C_{F343N,F438W,F814W}$  diagram of the observed RGB stars (left panel), the corresponding diagram for the sample of ASs (middle panel) and the selected PopA and PopB members (right panel). As in the case of NGC 121, the pseudo color-color diagram of NGC 416 clearly suggests the presence of two distinct groups of stars in this cluster (see also Dalessandro et al. 2016; Niederhofer et al. 2017a,b). On the other side the distribution of stars in NGC 339 and Lindsay 1 does not provide the same straightforward evidence. In all the cases, however, the observed  $C_{F343N,F438W,F814W}$  pseudo-color broadening is not compatible with the presence of a single stellar population.

#### 4. The relative helium content of multiple populations

The average color separation of PopA and PopB stars in a CMD is indicative of the different chemical content of the two stellar populations (Milone et al. 2015b). In particular, since optical bands are mainly sensitive to difference in helium content through the  $T_{\text{eff}}$  of the stars (Lagioia et al. 2018), CMDs obtained with a combinations of optical bands are ideal tools to study helium enrich-

ment in GCs. In order to quantify the helium abundance variations,  $\delta Y$ , we used the procedure already described in Milone et al. (2012b), based on the comparison of the observed color separation of a reference point along each RGB fiducial line with appropriate theoretical models.

The main steps of the procedure are summarized hereafter and have been applied to all the GCs studied in this work. We selected the ACS F814W filter as the reference band for all the color combinations,  $m_X - m_{F814W}$ , with  $X = F336W, F343N, F438W, F555W$ . Then, we determined the magnitude of the MS turn-off in the reference band by building the fiducial line of the MS stars, with the method of the naive-estimator (Silverman 1986): we divided the MS magnitude range into a grid of  $m_{F814W}^i$  points 0.025 mag apart. For each point we computed the median color, median magnitude and the 68th percentile ( $\sigma$ ) of the color distribution of all the stars in the interval  $m_{F814W}^i - 0.125 < m_{F814W}^j < m_{F814W}^i + 0.125$ . After performing, in each bin, a sigma-clipping rejection of all the stars with a distance from the median color greater than  $\sigma$ , we computed a new median color, magnitude and  $\sigma$ . We smoothed the resulting points with a boxcar average function and, finally, we linearly interpolated the new points along the MS magnitude interval. The point with the bluest color along the fiducial line was taken as the MS turn-off. In similar fashion, we built the fiducial line of the PopA and PopB stars in all the color combinations. In this case the analyzed magnitude range was divided into a grid of  $m_{F814W}^i$  points  $0.5/w$ , with  $w = 1$  for NGC 339, and  $w = 2$  for NGC 121, NGC 416 and Lindsay 1.

We note in passing that in the case of NGC 121, for which observation in the WFC3 F814W filter are also available, the choice of the latter as the reference band would not affect the conclusion of the present analysis. We indeed verified that the average difference between the ACS and WFC3 F814W magnitudes is consistent with zero for both PopA and PopB stars.

As an example, the fiducial lines of the PopA and PopB stars (represented as light red and light blue points, respectively) of NGC 121 are shown in Figure 4, where each panel displays a specific color combination. The dots along each fiducial line mark the points  $m_{F814W}^j = m_{F814W}^{TO} - (2 + 0.2 \cdot j)$  with  $j = 0, 1, 2, \dots, 11$ , while the horizontal dot-

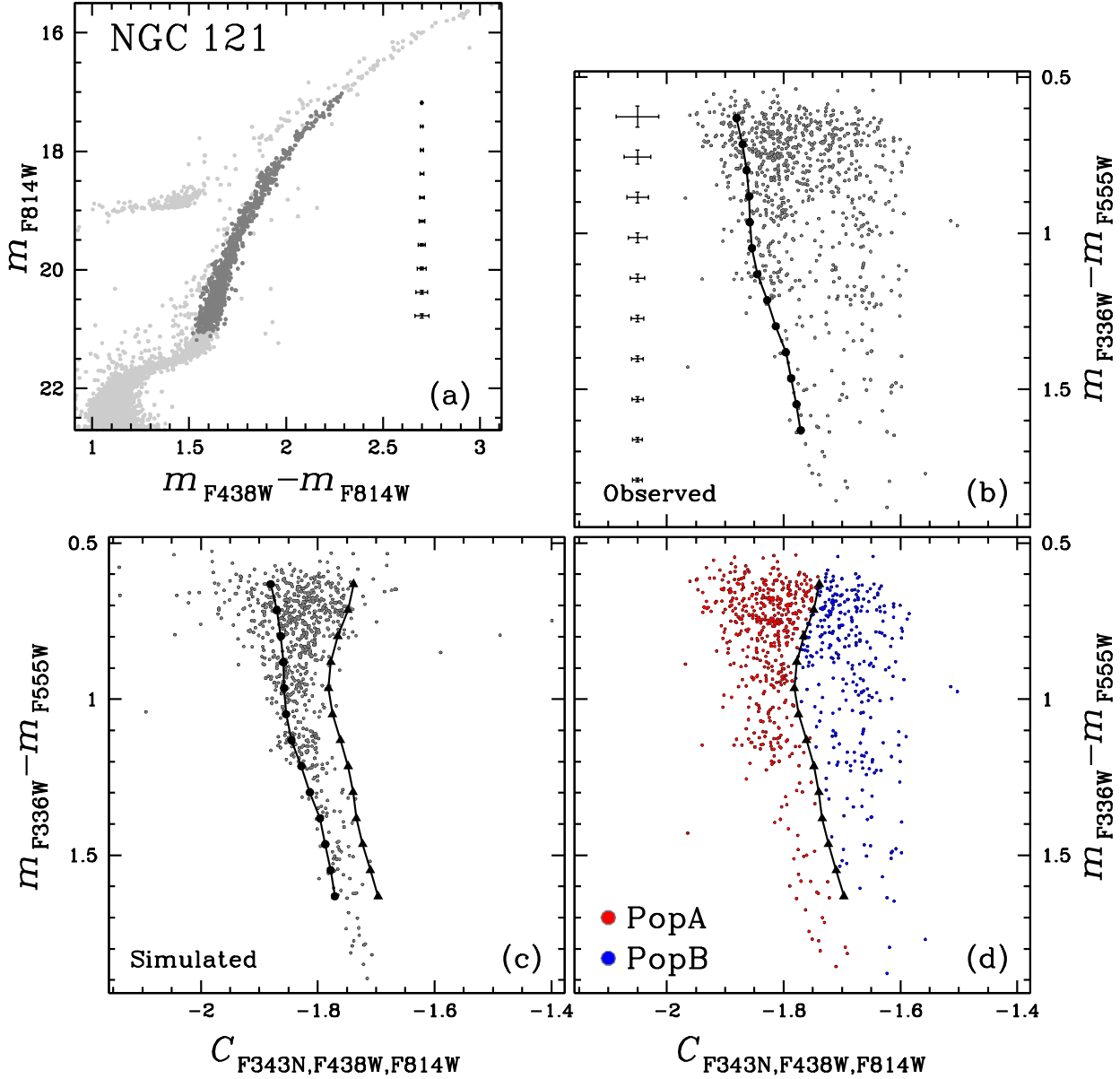


Fig. 2.— Selection of the two main stellar populations of NGC 121. *Panel (a)*: the cluster RGB members are represented by the dark-gray points in the  $m_{F814W}$  vs.  $m_{F438W} - m_{F814W}$  CMD. The error bars indicate the typical photometric uncertainties of the RGB stars as a function of the magnitude. *Panel (b)*:  $m_{F336W} - m_{F555W}$  vs.  $C_{F343N,F438W,F814W}$  pseudo color-color diagram of the observed RGB members. The black dots, connected by the solid line, mark the 10th percentile of the  $C_{F343N,F438W,F814W}$  pseudo-color distribution of the stars along the  $m_{F336W} - m_{F555W}$  direction. The error bars represent the typical color uncertainties as a function of the vertical coordinate. *Panel (c)*: same pseudo color-color diagram as in panel (b) but for the RGB ASs. The black dots and triangles mark, respectively, the 10th and 98th percentile of the ASs  $C_{F343N,F438W,F814W}$  pseudo-color distribution. *Panel (d)*: the ASs 98th percentile distribution divides the observed RGB stars into two groups, named PopA (red points) and PopB (blue points).

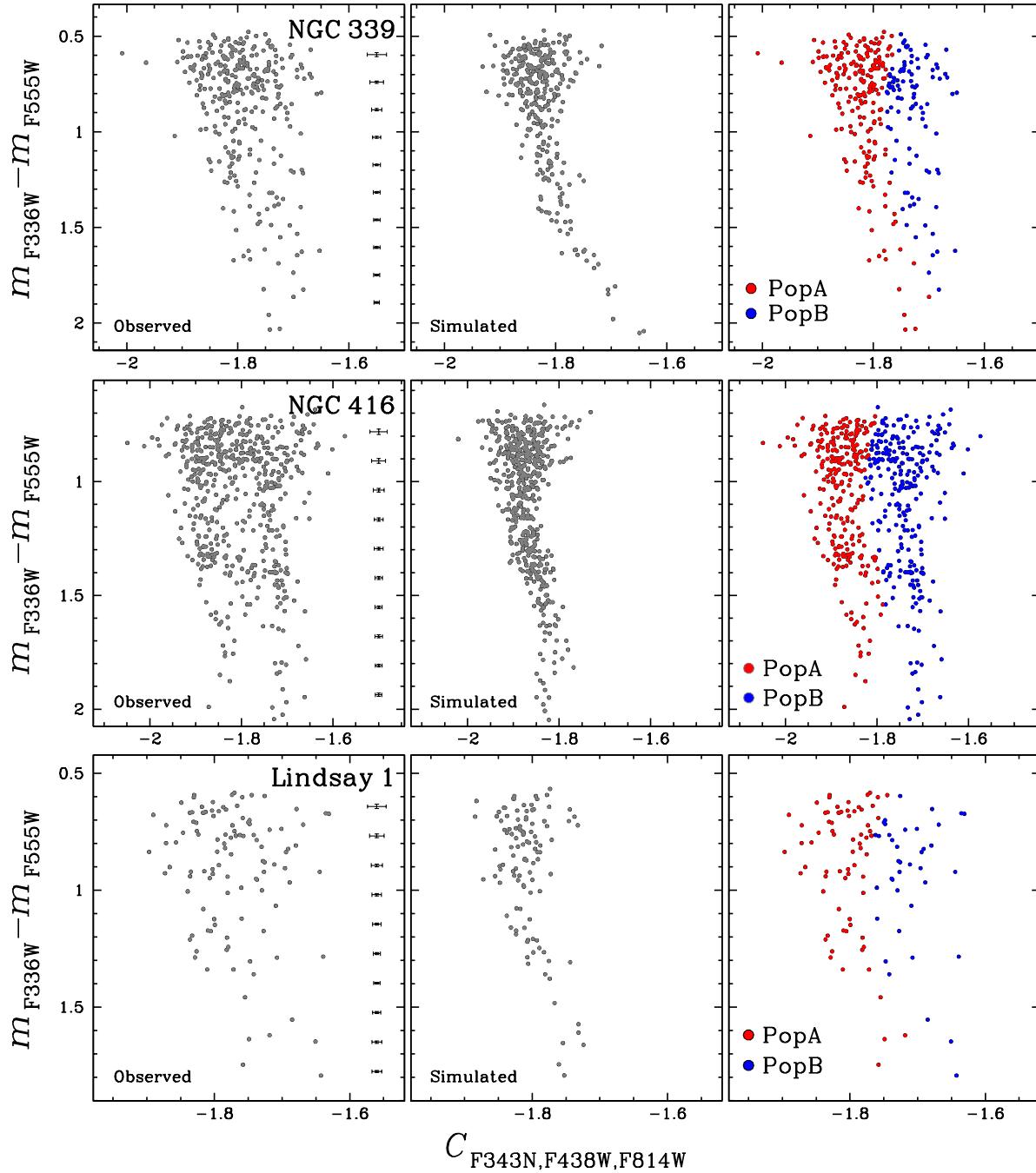


Fig. 3.— *Left panels:*  $m_{F336W} - m_{F555W}$  vs  $C_{F343N,F438W,F814W}$  pseudo color-color diagram for the observed RGB members of NGC 339, NGC 416 and Lindsay 1. The error bars represent the typical color uncertainties as a function of the  $m_{F336W} - m_{F555W}$  color; *Middle panels:* pseudo color-color diagram for the RGB ASs of each cluster. *Right panels:* selection of PopA and PopB stars in each cluster.

ted line marks the reference magnitude  $m_{F814W}^{CUT} = m_{F814W}^{TO} - 2.5$ . In each panel, the color difference relative to the color of the PopA fiducial point, at the reference magnitude, is plotted in the inset. The value of the color separation,  $\Delta\text{color} = m_X - m_{F814W}$ , is also reported with the associated error, obtained as the sum in quadrature of the standard error of the color of the PopA and PopB fiducial points, represented by the corresponding error bar in the plot.

The four panels in Figure 5 show, for each cluster, the trend of the color separation as a function of the central wavelength of the five filters used in this work. By construction the color separation is zero in F814W band. The error bar associated to each point has been obtained as the sum in quadrature of the standard errors of the color of the corresponding PopA and PopB fiducial line points. We observe an overall comparable trend for all the clusters, with differences attaining positive values in the UV-optical colors  $m_{F336W} - m_{F814W}$  and  $m_{F343N} - m_{F814W}$  and negative values in the optical colors  $m_{F438W} - m_{F814W}$  and  $m_{F555W} - m_{F814W}$ , with the exception of Lindsay 1 where the difference in  $m_{F555W} - m_{F814W}$  is slightly positive but compatible with zero within the errors. We also notice a large variation of the color difference values in correspondence of the narrow bandwidth filter  $F343N$ , ranging from 0.051 mag for NGC 339 to 0.102 for NGC 121.

As already shown in Milone et al. (2012b), the observed trends derive from the combined effect of the spectral response of the adopted filters and the chemical properties of the stellar populations. GC stars with primordial composition (C-rich, N-poor, O-rich) are redder than stars with enhanced composition (C-poor, N-rich, O-poor) in pure optical colors. Conversely, the former are bluer than the latter in the  $m_{F336W} - m_{F814W}$  or  $m_{F343N} - m_{F814W}$  UV-optical colors, because the transmission curve of both the F336W and F343N filters encompasses the NH absorption band in the typical GC RGB stars (Niederhofer et al. 2017a). In particular the drop of stellar flux is enhanced in the narrowband filter F343N.

#### 4.1. Synthetic spectra

To estimate the relative abundance of C, N, O and He for the two main populations of each cluster, we compared the observed colors of the PopA

and PopB RGB fiducial lines with the colors derived from synthetic spectra, in close analogy with what we did in previous papers (e.g. Milone et al. 2012a; Milone 2015).

First, we selected four reference magnitude values,  $m_{F814W}^l$ , where  $l = 1, 2, 3, 4$ , such that  $m_{F814W}^1 = m_{F814W}^{TO} - 1.5^5$  and two adjacent points differ by  $-0.5$  mag. Then, we estimated the  $T_{\text{eff}}$  and gravity associated to each  $m_{F814W}^l$  PopA point, by using isochrones with primordial helium content,  $Y = 0.245 + 1.5 \cdot Z$ , taken from the Dartmouth Stellar Evolution Database (Dotter et al. 2007, 2008). The parameters of the best-fit isochrone that we found for each cluster are listed in Table 2. For each model, we assumed the alpha-element abundance provided in Glatt et al. (2008a,b). The metallicity of the selected model was obtained by best-fitting the cluster RGB. The age was chosen by selecting the central value between the two models fitting the upper and lower envelope of the upper MS and Sub-Giant Branch region of the CMD. The typical errors affecting our determinations are  $\pm 0.5$  Gyr and  $\pm 0.1$  dex. The reported values are consistent with those found by Glatt and collaborators.

We used these parameters to simulate the corresponding stellar spectrum (hereafter reference spectrum) in the wavelength range between 2,500 and 10,000 Å. We assumed for the reference spectrum chemical abundances  $[C/Fe] = -0.1$ ,  $[N/Fe] = 0.0$  and  $[O/Fe] = [\alpha/Fe]$ .

Then, we computed a grid of synthetic spectra (comparison spectra) with the same metallicity as the reference spectrum but with  $Y$  ranging from the primordial value to 0.28 in steps of 0.001,  $[C/Fe]$  from  $-0.1$  to  $-0.4$  dex,  $[N/Fe]$  from 0.0 to 0.8 dex, and  $[O/Fe]$  from the reference alpha abundance values,  $[\alpha/Fe]_{\text{ref}}$ , listed in Table 2 to  $[\alpha/Fe]_{\text{ref}} - 0.5$ , all in steps of 0.05 dex. Since helium content significantly affects the structure of a star, hence its temperature and gravity (see Dotter et al. 2015, for discussion), we assumed for the comparison spectra the atmospheric parameters derived from the corresponding helium-enhanced isochrone. Also, we assumed constant  $[\text{Fe}/\text{H}]$  and overall C+N+O content (hence, the effect of metallicity on the stellar structure is the same for both PopA and PopB stars), in close

<sup>5</sup>In the case of NGC 121 we used  $m_{F814W}^1 = m_{F814W}^{TO} - 2.0$

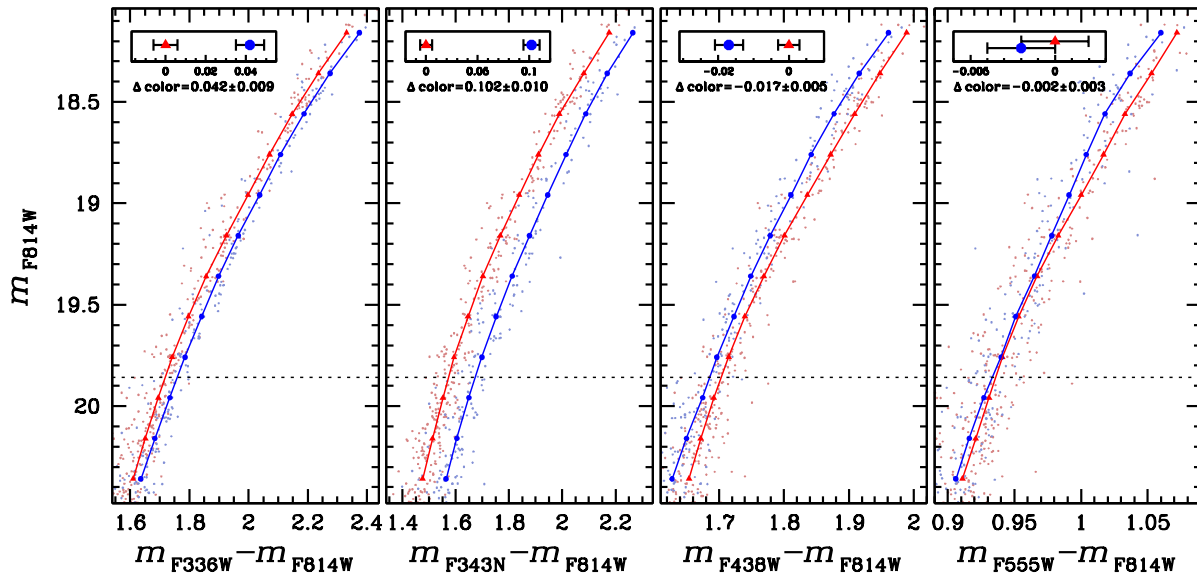


Fig. 4.— Fiducial line of the PopA (light red points) and PopB (light blue points) stars of NGC 121 in the  $m_{F814W}$  vs.  $m_X - m_{F814W}$  diagrams, with  $x = F336W, F343N, F438W, F555W$ . In each panel, the black dotted line is located at  $m_{F814W} = m_{F814W}^{TO} - 2.5$  and the difference between the color of the two fiducials at  $m_{F814W}^{CUT}$ , normalized to the PopA fiducial color, is plotted in the inset. The corresponding color difference is also indicated.

analogy with what done in previous papers (e.g. Dotter et al. 2015; Lagioia et al. 2018; Lee 2018; Milone et al. 2013, 2015b, 2018a). This assumption is supported by the fact that, so far, all the analyzed GCs, including NGC 121, do not show any evidence of metallicity and C+N+O variations. As an example, the cluster SGB morphology is consistent with mono-metallic stellar populations, as it does not show any evidence for splits and/or spreads, which are signatures of variation in the overall metallicity (e.g. Yong et al. 2009, 2014; Marino et al. 2009, 2012).

The spectra, obtained with ATLAS12 and SYNTHE codes (Castelli 2005; Kurucz 2005; Sbordone et al. 2007), have been integrated over the transmission curves of the UVIS/WFC3 and WFC/ACS filters used in this paper to derive the synthetic colors. The color differences between each comparison spectrum and the reference spectrum are compared to the observed color differences between PopB and PopA stars. We assumed, for the abundances of PopB stars, the content of C, N, O and He of the comparison

spectrum that provides the best fit with the observations.

Results are illustrated in Figure 6 for NGC 121. In the top panel we compare the reference spectrum and the comparison spectrum that best reproduces the relative colors of PopA and PopB stars with  $m_{F814W} = 19.864$  (2.5 mag brighter than  $m_{F814W}^{TO}$ ). The insets are zooms of the two spectra in the spectral regions of the F336W, F343N, F438W, F555W and F814W filters, while in the bottom panel we compare the observed color differences with those derived from the synthetic spectra.

It is important to notice that, since our analysis is based on the measurement of the relative color of fiducial points, the typical uncertainties affecting the determination of the best-fit isochrone parameters have a negligible impact on the derivation of the chemical variations between the two populations of each cluster. We verified that, for each cluster, a difference of  $\pm 0.5$  Gyr in age and  $\pm 0.1$  dex in metallicity of the adopted models results in an average difference on the estimate of helium

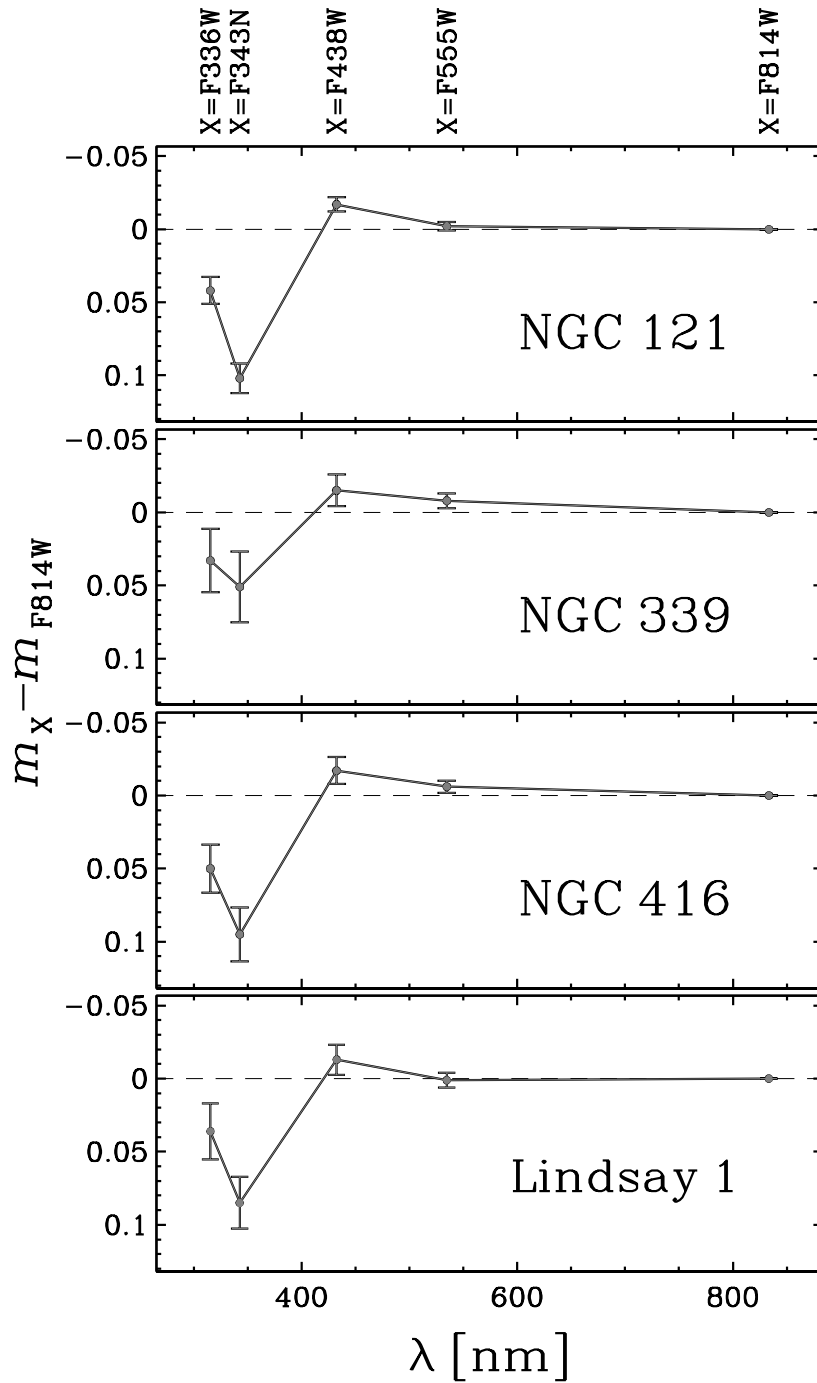


Fig. 5.— Color separation,  $m_X - m_{F814W}$ , with  $X = F336W, F343N, F438W, F555W, F814W$ , of the PopB and PopA fiducial lines at the reference magnitude for the four GCs studied in this work. The error bars associated to each point represent the standard error of the color difference.

variation equal to  $\langle \Delta(\delta Y) \rangle \lesssim 0.0001$ , which is negligible for our purposes.

In Tab. 2 we have reported, for each cluster, the parameters of the best-fit isochrone (age,  $[\text{Fe}/\text{H}]$ ,  $[\alpha/\text{Fe}]$ ) as well as the relative content of C, N, O and Y ( $\delta[\text{C}/\text{Fe}]$ ,  $\delta[\text{N}/\text{Fe}]$ ,  $\delta[\text{O}/\text{Fe}]$ ,  $\delta Y$ ) between the best-fit and the reference synthetic spectrum. We notice that for NGC 121, NGC 339 and NGC 416, PopB stars are more helium-rich than PopA stars of  $\sim 0.01$  in mass fraction, while both the stellar populations of Lindsay 1 have the same helium abundance within the errors.

In a recent paper, we identified the two main stellar populations, namely ‘1G’ and ‘2G’, in a large sample of Galactic GCs (Milone et al. 2017b) and inferred the average helium difference between 2G and 1G (Lagioia et al. 2018). In an attempt to compare the variation of helium of Milky Way and SMC clusters we overplotted, in Figure 7, the distribution of the  $\delta Y$  values in Tab. 2 (red histogram) to that obtained from the analysis of the RGBB by Lagioia et al. (2018, see their Fig.10, grey-shaded histogram). We see that the helium-enrichment in the four extragalactic GCs is compatible with that observed for most Galactic GCs ( $0.00 \lesssim \delta Y \lesssim +0.01$ ). Unfortunately, the selection of the two main stellar populations in the Galactic GCs is based on photometric diagrams (Milone et al. 2017b) and criteria different from those adopted in this paper. For this reason, we point out that this comparison is only indicative since the two groups of stars defined for each cluster in this work, namely PopA and PopB, do not necessarily correspond to the stellar populations ‘1G’ and ‘2G’ of the Galactic GCs.

## 5. Helium estimate from the RGB Bump

One of the most important evolutionary features of stellar populations older than  $\sim 1$  Gyr is the RGBB. It appears as a concentration of stars along the RGB in CMDs or, equivalently, as a prominent peak in the LF of RGB stars. The RGBB is produced by a temporary drop of the luminosity of red giant stars, during their ascent of the RGB, due to the increase in the gas opacity at the point in which the expanding hydrogen shell approaches the chemical discontinuity left behind by the deepest penetration of the convective envelope. Then, once the shell reaches the

discontinuity, the stellar luminosity starts again to increase monotonically (Sweigart et al. 1990; Cassisi et al. 2016). A direct consequence of such a mechanism is that the observational properties of the RGBB are directly related to the physical and chemical properties of the stars (Bono et al. 2001; Nataf 2014). For instance, variations in the chemical content of MPs in a GC will result in a brightness difference of the corresponding RGBBs. In particular, in visual bands this phenomenon is mostly connected to variation in helium abundance (Milone et al. 2015b; Lagioia et al. 2018).

As shown in the recent survey of Lagioia et al. (2018) on the RGBBs of multiple populations in Galactic GCs, the helium difference between the two main population of a cluster can be obtained with a method consisting of three main steps: the construction of the RGB LF for the measurement of the magnitude difference of the RGBB of the two populations in optical bands; the use of synthetic stars for the evaluation of the statistical significance of the peak detections; the comparison of observations with simulated CMDs obtained from appropriate theoretical models. We decided to apply this procedure for the estimate of the relative helium abundance of MPs in NGC 121, that is the only cluster among those analyzed in this paper for which the RGBB of PopA and PopB stars is visible. Indeed, owing to the low number of stars in the RGBB region, it was not possible to unambiguously determine the location of both the PopA and PopB RGBB for the cluster NGC 339 and Lindsay 1. Similarly, in the case of NGC 416, it was not possible to determine the RGBB location of PopB stars due to their flat distribution in the bump region.

### 5.1. The observed luminosity functions

The  $m_{F814W}$  vs.  $C_{F343N,F438W,F814W}$  CMD of the cluster is shown in the panel (a) of Figure 8. The black box, centered on the approximate location of the PopA and PopB RGBB, is extended over 0.8 mag along the  $m_{F814W}$  axis and includes the stars for which we determined the relative LF, plotted in panel (b). Both the PopA and PopB LFs, represented by the corresponding color histogram, were built by dividing the displayed magnitude range into a grid of  $m_{F814W}^k$  points 0.01 mag apart. For each point we counted the number of stars in the bin  $[m_{F814W}^k - 0.05, m_{F814W}^k + 0.05]$ .

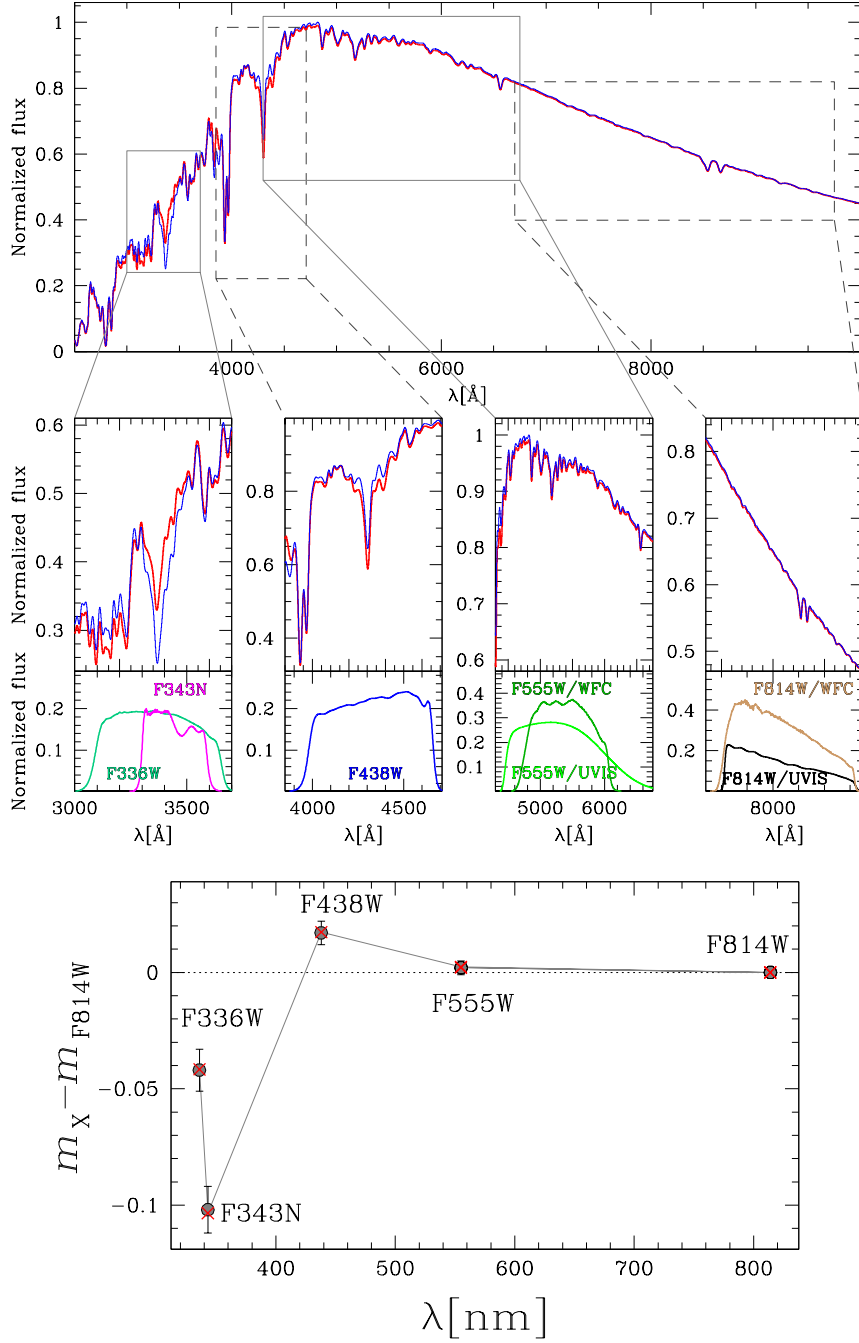


Fig. 6.— *Top panel*: reference spectrum (red;  $T_{\text{eff}}= 5260$  K,  $\log g= 2.90$ ) and comparison spectrum (blue;  $T_{\text{eff}}= 5274$  K,  $\log g= 2.90$ ) for the PopA and PopB stars of NGC 121. *Middle panels*: portion of the two spectra in the regions corresponding to the transmission curves of the filters used in this paper. *Bottom panel*: comparison between the color difference of the observed fiducial lines at the reference magnitude (gray dots) with the same quantity derived from synthetic spectra (red crosses).

TABLE 2  
PARAMETERS OF THE BEST-FIT ISOCHRONES (COLUMNS 2-6) AND CHEMICAL ABUNDANCE VARIATIONS  
(COLUMNS 7-10) BETWEEN POPA AND POPB STARS.

Cluster	$\mu_0$ (mag)	E(B-V) (mag)	age (Gyr)	[Fe/H] (dex)	[ $\alpha$ /Fe] (dex)	$\delta$ [C/Fe] (dex)	$\delta$ [N/Fe] (dex)	$\delta$ [O/Fe] (dex)	$\delta Y$
NGC 121	18.93	0.04	10.5	-1.30	0.20	-0.20	0.65	-0.25	$0.009 \pm 0.006$
NGC 339	18.85	0.06	6.5	-1.12	0.00	-0.10	0.50	0.00	$0.007 \pm 0.004$
NGC 416	18.96	0.09	6.0	-0.96	0.00	-0.15	0.60	0.00	$0.010 \pm 0.003$
Lindsay 1	18.80	0.04	8.0	-1.14	0.00	-0.20	0.45	-0.10	$0.000 \pm 0.004$

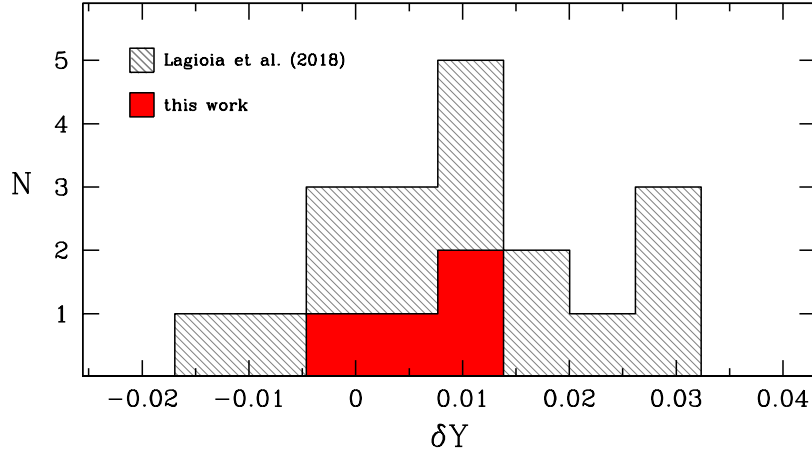


Fig. 7.— Comparison of the distribution of  $\delta Y$  values of the four SMC cluster analyzed in this paper (red histogram) with those found from the analysis of the RGBBs of the Galactic GCs (gray-shaded histogram) from Lagioia et al. (2018).

A smoother representation of each LF was obtained with a kernel density estimate of the magnitude distribution by employing a Gaussian kernel with  $\sigma = 0.04$  mag. The resulting probability distribution function has been overplotted as a green curve for the PopA LF and a yellow curve for the PopB LF. The corresponding maxima mark the location of the PopA and PopB RGBB while their magnitude difference,  $\Delta m^{(PopB, PopA)}$ , has been reported on the top of the panel.

The uncertainty associated to the  $\Delta m^{(PopB, PopA)}$  measurement was obtained as the sum in quadrature of the standard errors of the PopA and PopB RGBB magnitude. Each standard error corresponds the 68.27th percentile of the distribution of the estimates of RGBB magnitude obtained by performing 1000 bootstrapping tests on the corresponding population in the magnitude interval displayed in panel (b).

We found that the RGBB magnitude separation of NGC 121 in the WFC3 bands is:  $\Delta m_{F336W}^{(PopB, PopA)} = 0.020 \pm 0.020$ ,  $\Delta m_{F343N}^{(PopB, PopA)} = 0.075 \pm 0.032$ ,  $\Delta m_{F438W}^{(PopB, PopA)} = -0.069 \pm 0.024$ ,  $\Delta m_{F814W}^{(PopB, PopA)} = -0.070 \pm 0.021$ ; while in the ACS bands is:  $\Delta m_{F555W}^{(PopB, PopA)} = -0.067 \pm 0.027$ ,  $\Delta m_{F814W}^{(PopB, PopA)} = -0.052 \pm 0.017$ .

To quantify the significance of a RGBB detection, namely the probability that the peaks observed in the LFs are not the result of numerical fluctuations in the magnitude distribution of stars, we employed a statistical approach, based on the use of synthetic LFs. The method for the computation of the statistical significance has been described in detail in Lagioia et al. (2018), to which we refer the interested reader. By using this procedure we found that the statistical significance of the PopA and PopB RGBBs is higher than 99.3% in both the ACS and WFC3 F555W and F814W band.

## 5.2. Comparison with models

The last step for the determination of the helium variation between PopA and PopB stars in NGC 121 involves the comparison of the observed  $\Delta m_X^{(PopB, PopA)}$  with the corresponding best-match value obtained from appropriate theoretical models. To this purpose, we took advantage of the same set of isochrones used for the

analysis of synthetic spectra for this cluster (see Section 4.1).

We computed a grid of pairs of isochrones, one with standard helium content ( $Y \approx 0.25$ ) and the other with enhanced helium content, with a difference in helium abundance,  $\delta Y_i$ , ranging from 0.000 to 0.100 in steps of 0.001. For each pair of isochrones we simulated two CMDs, each one composed by 200,000 synthetic stars to account for observational errors in both color and magnitude. The slope of the LF of the helium standard and helium-enhanced synthetic CMD was assumed equal to that of the observed PopA and PopB LF, respectively. For each couple of synthetic CMDs, the estimate of  $\Delta m_i^{(PopB, PopA)}$  was obtained with the same procedure used for the observations. As already seen in Lagioia et al. (2018), C, N, O and He variation all contribute to produce the observed magnitude displacement between the two RGBBs. For this reason we computed, with the method described in Section 4.1, the quantity  $\Delta m_{X, CNO}^{(PopB, PopA)}$  ( $\Delta m_{F555W, CNO}^{(PopB, PopA)} = -0.0059$  mag,  $\Delta m_{F814W, CNO}^{(PopB, PopA)} = -0.0024$  mag), which indicates the contribution of C, N and O to the observed magnitude difference, and determined for each simulation, the quantity  $\Delta m_{i, X, He}^{(PopB, PopA)} = \Delta m_i^{(PopB, PopA)} - \Delta m_{X, CNO}^{(PopB, PopA)}$ . Finally we assumed the value of  $\delta Y_i$  providing  $\Delta m_{i, X, He}^{(PopB, PopA)} = \Delta m_X^{(PopB, PopA)} - \Delta m_{X, CNO}^{(PopB, PopA)}$ , as the best estimate of the helium content difference between PopB and PopA stars,  $\delta Y$ . We emphasize that we assumed for PopA and PopB the same metallicity in close analogy with what was done in similar work by Lagioia et al. (2018); Lee (2018); Milone et al. (2015b).

In Figure 9 we show the procedure for the estimate of  $\delta Y$  in the F814W band for NGC 121. In the left panels two isochrones, the red with  $Y = 0.247$  and the blue with  $Y = 0.271$ , corresponding to the best estimate of  $\delta Y_i$  for this cluster, have been overplotted to the corresponding synthetic CMDs. The helium-enhanced isochrone has been obtained by linearly interpolating the models with  $Y = 0.247$  and  $Y = 0.280$ . Age, [Fe/H] and  $[\alpha/Fe]$  of the adopted models are reported in the upper-left corner. In the right panel the corresponding synthetic LFs, normalized to their peak value, are shown together with the resulting best-matching

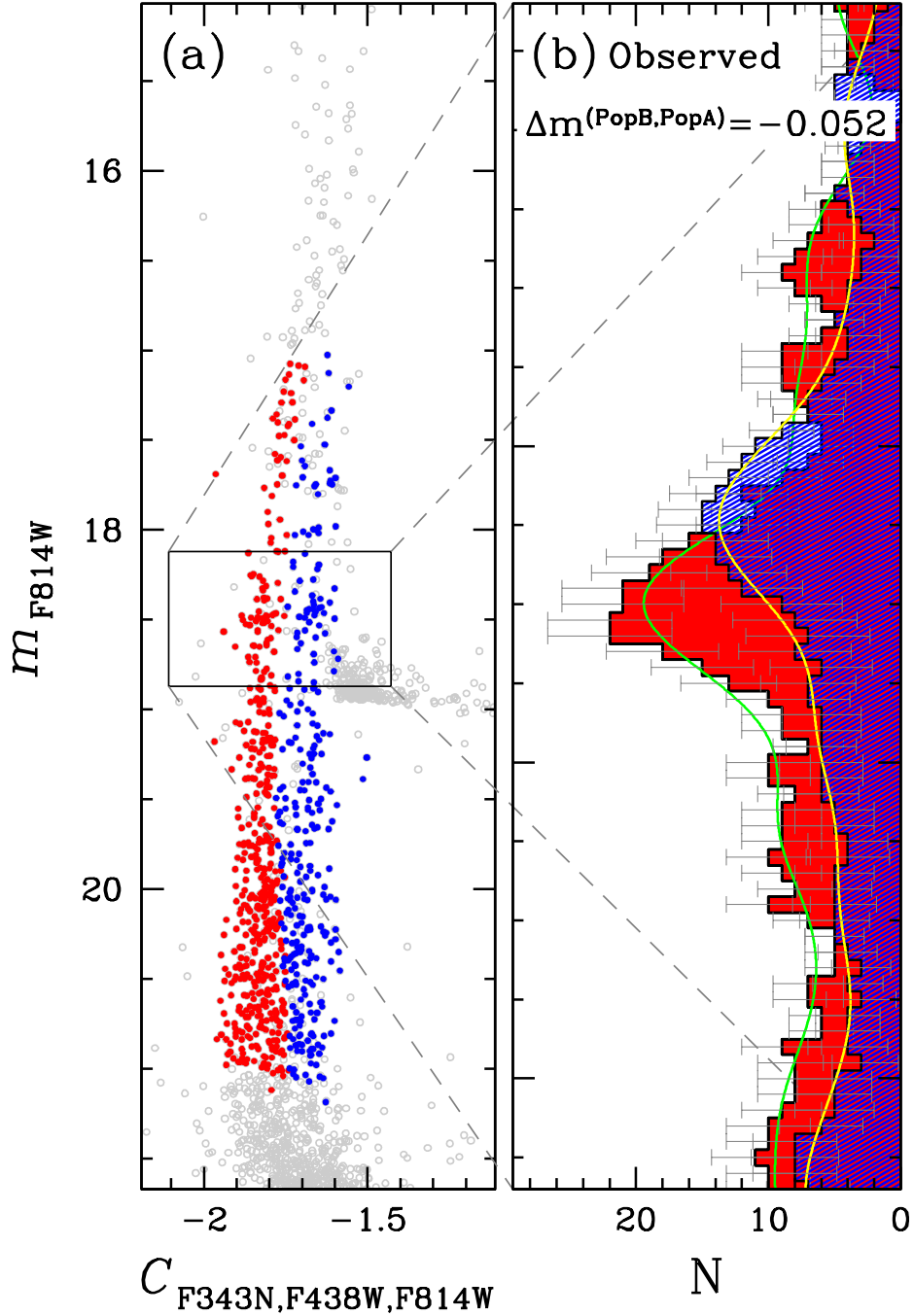


Fig. 8.— *Panel (a)*:  $m_{F814W}$  vs.  $C_{F343N,F438W,F814W}$  pseudo CMD of NGC 121. *Panel (b)*: LF of the PopA and PopB stars included in the black box plotted in the left panel. The gray error bars indicate the uncertainty relative to the star count of the stars in each histogram bin. The overlapped green and yellow curves indicate the kernel density estimate of the PopA and PopB magnitude distribution. The peak of each curve identifies the RGBB magnitude of the corresponding stellar population.

magnitude difference,  $\Delta m_i^{(PopB, PopA)}_{F814W, He} = -0.050$ .

We found that the corresponding  $\delta Y$  is  $0.024 \pm 0.011$ . Similarly, in F555W band, we found  $\delta Y = 0.028 \pm 0.014$ . Therefore, we considered the weighted mean of the two estimates,  $\delta Y = 0.026 \pm 0.009$ , as our best estimate of the helium content difference between the two populations.

Noticeably the relative helium abundance derived from the analysis of the RGBB is consistent with the value of  $\delta Y$  inferred from multiple RGBs at  $\sim 1.5\sigma$  level only.

## 6. Summary

In recent work, we introduced a new method to constrain the relative helium abundance of MPs in GCs from multi-band photometry of MS, RGB, and RGB bump stars and find that internal variations of helium are a distinctive feature of old Galactic GCs (e.g. Milone et al. 2015a). Specifically, from the study of a large sample of Galactic GCs, we found that, on average, second-population stars (2G) are enhanced by  $\sim 0.01$  in helium mass fraction with respect to the first population stars (1G, Lagioia et al. 2018; Milone et al. 2018a).

These results provide strong constraints on the physical processes responsible for the formation of the MPs (e.g. Renzini et al. 2015; D’Antona et al. 2016; Chantereau et al. 2017; Gieles et al. 2018).

In this work we exploited multi-band *HST* photometry in four SMC GCs, namely NGC 121, NGC 339, NGC 416 and Lindsay 1, to investigate, for the first time, the internal helium variations by using RGB stars. We confirm previous results by Niederhofer et al. (2017a,b) that the CMDs of these clusters are not consistent with a simple population and identified the two main populations, PopA and PopB, along the RGB of each cluster.

From the comparison of the observed colors of the PopA and PopB stars with synthetic spectra with appropriate chemical composition we find that PopB are on average enhanced in helium by  $\sim 0.007$  with respect to PopA stars, similarly to what is observed in Galactic GCs. Specifically we obtained  $\delta Y = 0.009 \pm 0.006$  for NGC 121,  $\delta Y = 0.007 \pm 0.004$  for NGC 339,  $\delta Y = 0.010 \pm 0.003$  for NGC 416 and  $\delta Y = 0.000 \pm 0.004$  for Lindsay 1.

We also provided estimates for the internal variations in the abundance of carbon, nitrogen, and oxygen and find that PopB are enhanced in N by  $\sim 0.4 - 0.6$  dex, and depleted in C and O by  $\sim 0.1 - 0.2$  dex and  $\sim 0.0 - 0.3$  dex, respectively, with respect to PopA stars. In the case of NGC 121 we identified the RGB bumps of the two main populations and exploited their luminosities to infer the relative helium content. We find that PopB stars are enhanced in helium by  $\sim 0.026$  with respect to PopA, in agreement at  $\sim 1.5\sigma$  level with the value inferred from the colors of RGB stars.

A variation of helium content among the stars in NGC 121 was already suggested by Niederhofer et al. (2017a), who tried to qualitatively reproduce the shape of the cluster HB by simulating a synthetic population of stars with a spread of helium mass content of  $\Delta Y = 0.025$ .

Noticeably, Hollyhead et al. (2017) measured the CN and CH band strength from low-resolution spectroscopy of 16 RGB stars in Lindsay 1, and concluded that six stars are enhanced in [N/Fe] by  $\sim 0.7$  with respect to the majority of analyzed stars. All the analyzed stars share almost constant carbon abundance. Our photometric observations of Lindsay 1 indicate that PopB stars are enhanced in nitrogen by  $\sim 0.45$  dex with respect to PopA stars thus providing further evidence of significant nitrogen variations in this cluster. In contrast, our work suggests that nitrogen anticorrelates with carbon, similarly to what is observed in Galactic GCs. However, caution must be used when comparing the results of this paper and those by Hollyhead et al. (2017). Indeed the two groups of stars selected in this paper, namely PopA and PopB, do not necessarily correspond to the sample of N-rich and N-poor stars by Hollyhead and collaborators.

Most of the studies on MPs are focused on Galactic GCs older than  $\sim 11$  Gyr. The finding of MPs in Magellanic Clouds GCs with ages between  $\sim 6$  and  $11$  Gyr provide further information on the multiple-population phenomenon. These clusters, indeed, allow to investigate MPs to early stages of the cluster formation as well as to understand the impact of a different environments.

Our paper provides evidence that the two main populations of four  $\sim 6$  and  $11$  Gyr old GCs differ in helium by  $\sim 0.007$ , in close analogy with what is observed in old Galactic GCs. The more helium-

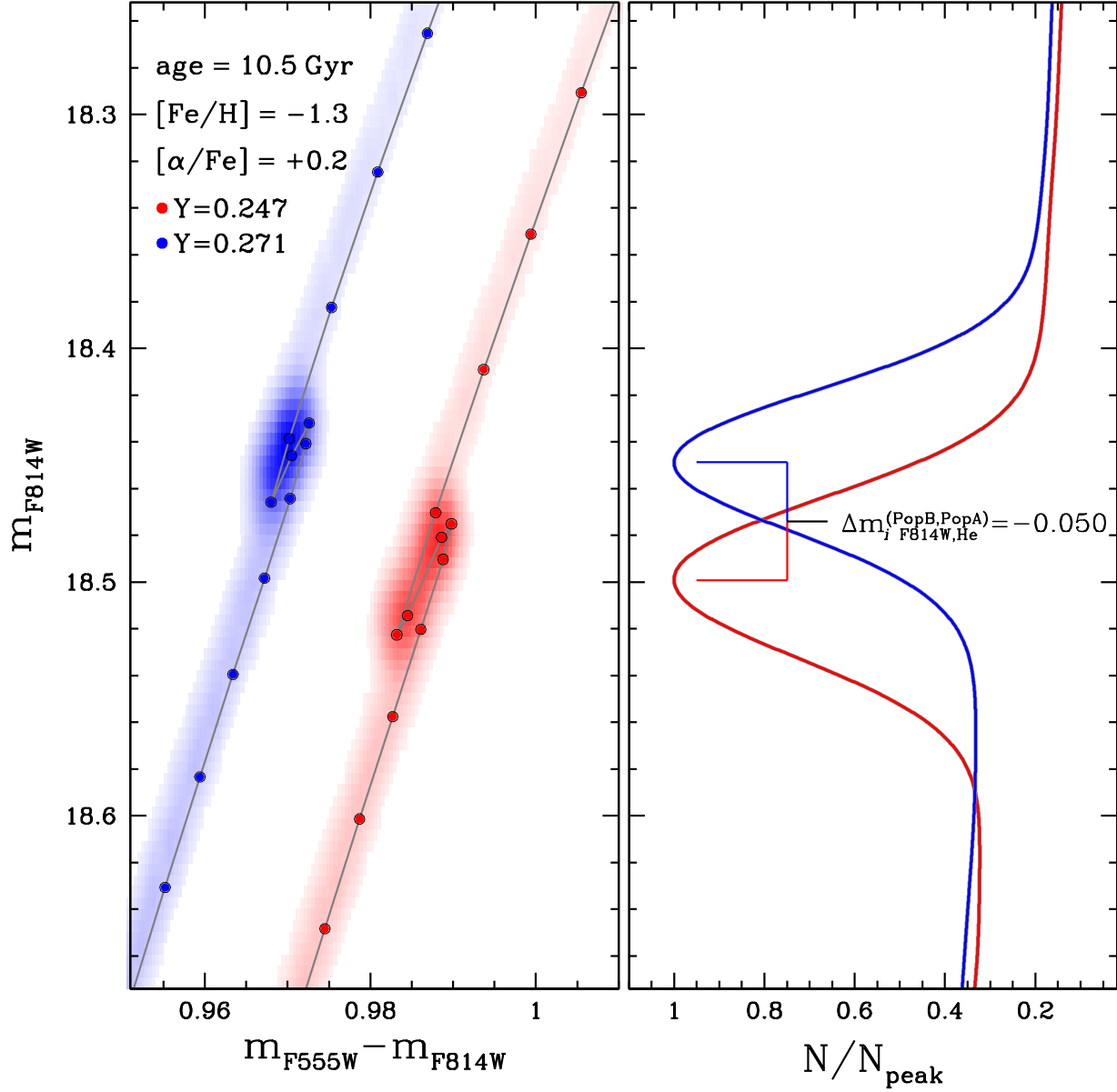


Fig. 9.— *Left panel*: best-fit isochrones for the PopA and PopB stars of NGC 121. The red and blue points mark, respectively, the location of the model with  $Y = 0.247$  and  $Y = 0.271$  in the  $m_{F814W}$  vs  $m_{F555W} - m_{F814W}$  CMD. The red and blue shaded areas represent the Hess diagram of the synthetic CMDs obtained from the two isochrones. *Right panel*: kernel density estimate of the magnitude distribution of the two synthetic stellar populations. The magnitude difference between the two synthetic RGB Bumps is indicated.

rich stars in our analyzed SMC clusters are also more N-rich and more C-O-poor than stars with primordial helium. These results are consistent with a scenario where MPs in old Galactic GCs and younger SMC clusters share similar properties.

This work has received funding from the European Research Council (ERC) under the European Union's Horizon 2020 research innovation programme (Grant Agreement ERC-StG 2016, No 716082 'GALFOR', PI: Milone), and the European Union's Horizon 2020 research and innovation programme under the Marie Skłodowska-Curie (Grant Agreement No 797100, beneficiary: Marino). APM acknowledges support from MIUR through the the FARE project R164RM93XW 'SEMPLICE'.

HST (ACS, WFC3)

## REFERENCES

- Anderson, J., & Bedin, L. R. 2010, *PASP*, 122, 1035, doi: 10.1086/656399
- Anderson, J., & King, I. R. 2006, PSFs, Photometry, and Astronomy for the ACS/WFC, Tech. rep.
- Anderson, J., Sarajedini, A., Bedin, L. R., et al. 2008, *AJ*, 135, 2055, doi: 10.1088/0004-6256/135/6/2055
- Bastian, N., Lamers, H. J. G. L. M., de Mink, S. E., et al. 2013, *MNRAS*, 436, 2398, doi: 10.1093/mnras/stt1745
- Bastian, N., Niederhofer, F., Kozhurina-Platais, V., et al. 2016, *MNRAS*, 460, L20, doi: 10.1093/mnrasl/slw067
- Bedin, L. R., Cassisi, S., Castelli, F., et al. 2005, *MNRAS*, 357, 1038, doi: 10.1111/j.1365-2966.2005.08735.x
- Behr, B. B. 2003, *ApJS*, 149, 67, doi: 10.1086/377509
- Bellini, A., Anderson, J., & Bedin, L. R. 2011, *PASP*, 123, 622, doi: 10.1086/659878
- Bellini, A., Anderson, J., Bedin, L. R., et al. 2017, *ApJ*, 842, 6, doi: 10.3847/1538-4357/aa7059
- Bertelli, G., Nasi, E., Girardi, L., et al. 2003, *AJ*, 125, 770, doi: 10.1086/345961
- Bono, G., Cassisi, S., Zoccali, M., & Piotto, G. 2001, *ApJ*, 546, L109, doi: 10.1086/318866
- Cassisi, S., degl'Innocenti, S., & Salaris, M. 1997, *MNRAS*, 290, 515, doi: 10.1093/mnras/290.3.515
- Cassisi, S., Salaris, M., & Pietrinferni, A. 2016, *A&A*, 585, A124, doi: 10.1051/0004-6361/201527412
- Cassisi, S., Salaris, M., Pietrinferni, A., & Hyder, D. 2017, *MNRAS*, 464, 2341, doi: 10.1093/mnras/stw2579
- Castelli, F. 2005, *Memorie della Societa Astronomica Italiana Supplementi*, 8, 25
- Chantereau, W., Charbonnel, C., & Meynet, G. 2017, *A&A*, 602, A13, doi: 10.1051/0004-6361/201730537
- Dalessandro, E., Lapenna, E., Mucciarelli, A., et al. 2016, *ApJ*, 829, 77, doi: 10.3847/0004-637X/829/2/77
- D'Antona, F., Di Criscienzo, M., Decressin, T., et al. 2015, *MNRAS*, 453, 2637, doi: 10.1093/mnras/stv1794
- D'Antona, F., Vesperini, E., D'Ercole, A., et al. 2016, *MNRAS*, 458, 2122, doi: 10.1093/mnras/stw387
- Decressin, T., Meynet, G., Charbonnel, C., Prantzos, N., & Ekström, S. 2007, *A&A*, 464, 1029, doi: 10.1051/0004-6361:20066013
- D'Ercole, A., Vesperini, E., D'Antona, F., McMillan, S. L. W., & Recchi, S. 2008, *MNRAS*, 391, 825, doi: 10.1111/j.1365-2966.2008.13915.x
- Dotter, A., Chaboyer, B., Jevremović, D., et al. 2007, *AJ*, 134, 376, doi: 10.1086/517915
- . 2008, *ApJS*, 178, 89, doi: 10.1086/589654
- Dotter, A., Ferguson, J. W., Conroy, C., et al. 2015, *MNRAS*, 446, 1641, doi: 10.1093/mnras/stu2170

- Dupree, A. K., Strader, J., & Smith, G. H. 2011, *ApJ*, 728, 155, doi: 10.1088/0004-637X/728/2/155
- Gaia Collaboration, Brown, A. G. A., Valenari, A., et al. 2016, *A&A*, 595, A2, doi: 10.1051/0004-6361/201629512
- Gieles, M., Charbonnel, C., Krause, M. G. H., et al. 2018, *MNRAS*, 478, 2461, doi: 10.1093/mnras/sty1059
- Gilliland, R. 2010, in *Hubble after SM4. Preparing JWST*, 63
- Gilliland, R. L. 2004, *ACS CCD Gains, Full Well Depths, and Linearity up to and Beyond Saturation*, Tech. rep.
- Glatt, K., Grebel, E. K., Sabbi, E., et al. 2008a, *AJ*, 136, 1703, doi: 10.1088/0004-6256/136/4/1703
- Glatt, K., Gallagher, III, J. S., Grebel, E. K., et al. 2008b, *AJ*, 135, 1106, doi: 10.1088/0004-6256/135/4/1106
- Goudfrooij, P., Puzia, T. H., Kozhurina-Platais, V., & Chandar, R. 2009, *AJ*, 137, 4988, doi: 10.1088/0004-6256/137/6/4988
- . 2011, *ApJ*, 737, 3, doi: 10.1088/0004-637X/737/1/3
- Gratton, R. G., Carretta, E., & Bragaglia, A. 2012, *Astronomy and Astrophysics Review*, 20, 50, doi: 10.1007/s00159-012-0050-3
- Grundahl, F., Catelan, M., Landsman, W. B., Stetson, P. B., & Andersen, M. I. 1999, *ApJ*, 524, 242, doi: 10.1086/307807
- Hollyhead, K., Kacharov, N., Lardo, C., et al. 2017, *MNRAS*, 465, L39, doi: 10.1093/mnras/1/slw179
- Johnson, J. A., Bolte, M., Stetson, P. B., Hesser, J. E., & Somerville, R. S. 1999, *ApJ*, 527, 199, doi: 10.1086/308066
- Kraft, R. P. 1994, *Publications of the Astronomical Society of the Pacific*, 106, 553, doi: 10.1086/133416
- Kurucz, R. L. 2005, *Memorie della Societa Astronomica Italiana Supplementi*, 8, 14
- Lagioia, E. P., Milone, A. P., Marino, A. F., et al. 2018, *MNRAS*, 475, 4088, doi: 10.1093/mnras/sty083
- Lee, J.-W. 2015, *The Astrophysical Journal Supplement Series*, 219, 7, doi: 10.1088/0067-0049/219/1/7
- . 2017, *ApJ*, 844, 77, doi: 10.3847/1538-4357/aa7b8c
- . 2018, *The Astrophysical Journal Supplement Series*, 238, 24, doi: 10.3847/1538-4365/aadcad
- Mackey, A. D., & Broby Nielsen, P. 2007, *MNRAS*, 379, 151, doi: 10.1111/j.1365-2966.2007.11915.x
- Mackey, A. D., Broby Nielsen, P., Ferguson, A. M. N., & Richardson, J. C. 2008, *ApJ*, 681, L17, doi: 10.1086/590343
- Mackey, A. D., & Gilmore, G. F. 2004, *MNRAS*, 352, 153, doi: 10.1111/j.1365-2966.2004.07908.x
- Marino, A. F., Milone, A. P., Piotto, G., et al. 2009, *A&A*, 505, 1099, doi: 10.1051/0004-6361/200911827
- Marino, A. F., Villanova, S., Piotto, G., et al. 2008, *A&A*, 490, 625, doi: 10.1051/0004-6361:200810389
- Marino, A. F., Milone, A. P., Sneider, C., et al. 2012, *A&A*, 541, A15, doi: 10.1051/0004-6361/201118381
- Marino, A. F., Milone, A. P., Przybilla, N., et al. 2014, *MNRAS*, 437, 1609, doi: 10.1093/mnras/stt1993
- Marino, A. F., Milone, A. P., Karakas, A. I., et al. 2015, *MNRAS*, 450, 815, doi: 10.1093/mnras/stv420
- Marino, A. F., Milone, A. P., Yong, D., et al. 2017, *ApJ*, 843, 66, doi: 10.3847/1538-4357/aa7852
- Martocchia, S., Cabrera-Ziri, I., Lardo, C., et al. 2018, *MNRAS*, 473, 2688, doi: 10.1093/mnras/stx2556
- Milone, A. P. 2015, *MNRAS*, 446, 1672, doi: 10.1093/mnras/stu2198

- Milone, A. P., Bedin, L. R., Piotto, G., & Anderson, J. 2009, *A&A*, 497, 755, doi: 10.1051/0004-6361/200810870
- Milone, A. P., Marino, A. F., D’Antona, F., et al. 2016, *MNRAS*, 458, 4368, doi: 10.1093/mnras/stw608
- Milone, A. P., Marino, A. F., Piotto, G., et al. 2012a, *ApJ*, 745, 27, doi: 10.1088/0004-637X/745/1/27
- Milone, A. P., Piotto, G., Bedin, L. R., et al. 2012b, *ApJ*, 744, 58, doi: 10.1088/0004-637X/744/1/58
- Milone, A. P., Marino, A. F., Piotto, G., et al. 2013, *ApJ*, 767, 120, doi: 10.1088/0004-637X/767/2/120
- . 2015a, *MNRAS*, 447, 927, doi: 10.1093/mnras/stu2446
- . 2015b, *ApJ*, 808, 51, doi: 10.1088/0004-637X/808/1/51
- Milone, A. P., Marino, A. F., D’Antona, F., et al. 2017a, *MNRAS*, 465, 4363, doi: 10.1093/mnras/stw2965
- Milone, A. P., Piotto, G., Renzini, A., et al. 2017b, *MNRAS*, 464, 3636, doi: 10.1093/mnras/stw2531
- Milone, A. P., Marino, A. F., Renzini, A., et al. 2018a, *MNRAS*, 481, 5098, doi: 10.1093/mnras/sty2573
- Milone, A. P., Marino, A. F., Di Criscienzo, M., et al. 2018b, *MNRAS*, doi: 10.1093/mnras/sty661
- Moehler, S., Sweigart, A. V., Landsman, W. B., Hammer, N. J., & Dreizler, S. 2004, *A&A*, 415, 313, doi: 10.1051/0004-6361:20034505
- Monelli, M., Milone, A. P., Stetson, P. B., et al. 2013, *MNRAS*, 431, 2126, doi: 10.1093/mnras/stt273
- Monelli, M., Milone, A. P., Fabrizio, M., et al. 2014, *ApJ*, 796, 90, doi: 10.1088/0004-637X/796/2/90
- Mucciarelli, A., Dalessandro, E., Ferraro, F. R., Origlia, L., & Lanzoni, B. 2014, *ApJ*, 793, L6, doi: 10.1088/2041-8205/793/1/L6
- Mucciarelli, A., Origlia, L., Ferraro, F. R., & Pancino, E. 2009, *ApJ*, 695, L134, doi: 10.1088/0004-637X/695/2/L134
- Mucciarelli, A., Cristallo, S., Brocato, E., et al. 2011, *MNRAS*, 413, 837, doi: 10.1111/j.1365-2966.2010.18167.x
- Nataf, D. M. 2014, *MNRAS*, 445, 3839, doi: 10.1093/mnras/stu1974
- Niederhofer, F., Bastian, N., Kozhurina-Platais, V., et al. 2017a, *MNRAS*, 464, 94, doi: 10.1093/mnras/stw2269
- . 2017b, *MNRAS*, 465, 4159, doi: 10.1093/mnras/stw3084
- Pasquini, L., Mauas, P., Käuff, H. U., & Cacciari, C. 2011, *A&A*, 531, A35, doi: 10.1051/0004-6361/201116592
- Renzini, A. 2017, *MNRAS*, 469, L63, doi: 10.1093/mnrasl/slx057
- Renzini, A., D’Antona, F., Cassisi, S., et al. 2015, *MNRAS*, 454, 4197, doi: 10.1093/mnras/stv2268
- Sabbi, E., Lennon, D. J., Anderson, J., et al. 2016, *ApJS*, 222, 11, doi: 10.3847/0067-0049/222/1/11
- Sbordone, L., Bonifacio, P., Buonanno, R., et al. 2007, *A&A*, 465, 815, doi: 10.1051/0004-6361:20066385
- Schaerer, D., & Charbonnel, C. 2011, *MNRAS*, 413, 2297, doi: 10.1111/j.1365-2966.2011.18304.x
- Silverman, B. W. 1986, *Density estimation for statistics and data analysis*
- Sweigart, A. V., Greggio, L., & Renzini, A. 1990, *ApJ*, 364, 527, doi: 10.1086/169434
- Villanova, S., Piotto, G., & Gratton, R. G. 2009, *A&A*, 499, 755, doi: 10.1051/0004-6361/200811493

Yong, D., Grundahl, F., D'Antona,  
F., et al. 2009, ApJ, 695, L62,  
doi: 10.1088/0004-637X/695/1/L62

Yong, D., Roederer, I. U., Grundahl,  
F., et al. 2014, MNRAS, 441, 3396,  
doi: 10.1093/mnras/stu806